

Analytical interatomic potential for modeling non-equilibrium processes in the W–C–H system

N. Juslin,¹ P. Erhart,² P. Träskelin,¹ J. Nord,¹ K. O. E. Henriksson,¹ E. Salonen,^{1,3} K. Nordlund,¹ and K. Albe²

¹ Accelerator Laboratory, P.O. Box 43, FIN-00014 University of Helsinki, Finland

² Technische Universität Darmstadt, Institut für Materialwissenschaft, Petersenstr. 23, D-64287 Darmstadt, Germany

³ Laboratory of Physics and Helsinki Institute of Physics,
P.O. Box 1100, FIN-02015 Helsinki University of Technology, Finland

(Dated: June 14, 2005)

A reactive interatomic potential based on an analytic bond-order scheme is developed for the ternary system W-C-H. The model combines Brenner's hydrocarbon potential with parameter sets for W-W, W-C and W-H interactions and is adjusted to materials properties of reference structures with different local atomic coordinations including tungsten carbide, W-H molecules as well as H dissolved in bulk W. The potential has been tested in various scenarios, like surface, defect, and melting properties, none of which were considered in the fitting. The intended area of application is simulations of hydrogen and hydrocarbon interactions with tungsten, that have a crucial role in fusion reactor plasma-walls. Furthermore, this study shows that the angular dependent bond-order scheme can be extended to second-nearest neighbor interactions, which are relevant in body-centered cubic metals. Moreover, it provides a possibly general route for modeling metal carbides.

PACS numbers: 34.20.Cf, 81.05.Bx, 81.05.Je, 02.70.Ns

I. INTRODUCTION

Tungsten carbide exhibits extraordinary mechanical and thermal properties including high strength and low ductility at high temperatures. For practical applications it is usually alloyed with softer metals, like cobalt, which improves ductility while maintaining the high temperature strength^{1,2}. Because of its high wear resistance WC is widely used as coating material in tools, ball mills, extrusion dies, rollers and drills. Moreover, it can be used to catalyze oxidation of hydrogen^{3,4} and may act as a catalyst for boron nitride nanotube growth⁵.

A peculiar application of tungsten and tungsten carbide is its intended use as wall material in fusion reactors. The divertor (bottom) region of the first wall of the ITER fusion reactor is designed to be mostly tungsten but with some carbon layers on those parts subject to the highest heat load⁶. Hence W-C interfaces will be present in the reactor first wall by default. Furthermore, during the reactor operation the whole divertor will be subject to intense bombardment by low-energy (1–100 eV) H isotopes, giving rise to small hydrocarbon molecule erosion as well as H bubble formation^{7–9}. The eroded hydrocarbons are further known to drift in the reactor and form films on other parts of the first wall, including the W parts¹⁰.

For most practical applications it is decisive to understand and predict the materials properties and performance under processing and service conditions, like mechanical loading or irradiation. At this point atomic scale simulations that include detailed structural information are the most attractive tool. Computer simulations on large scales, with ensemble sizes in the multi-million atom regime are, however, only feasible if an appropriate and computationally efficient description of interatomic interactions is available.

Realistic analytical potentials that describe variations of the local chemical environment have become available over the last two decades for a number of different materials. Pure metals and their alloys have been described in different contexts by the embedded atom method (EAM) of Daw and

Baskes¹¹. At the same time a variety of mathematically equivalent schemes emerged. Among them, the Finnis-Sinclair type potentials¹² based on the second-moment approximation have been widely used for modeling body-centered cubic (bcc) metals and their alloys. In case of transition metals with partially filled d-bands, however, angular force terms are needed to correctly describe surface properties, point defects and structural stabilities. In case of tungsten Moriarty¹³ and Carlsson¹⁴ were reporting theoretical models to treat such systems, and an application of the fourth moment approximation of the tight binding scheme was presented by Xu and Adams¹⁵ for modelling tungsten surfaces. Recently, Baskes' modified embedded atom method that includes angular dependent electron densities has been extended to a second nearest neighbor-model by Lee *et al.* for describing bcc metals.

As it comes to carbide forming materials, very few interatomic potentials are available for large-scale atomistic simulations. The only exception is silicon carbide that has been extensively studied in the past^{16–19}. Recently, Li *et al.* derived a potential for Zr-C based on an extended second-moment scheme²⁰, that includes angular dependencies in its screening decay factor. An alternative approach for modelling metal carbon interaction in Pt-C was chosen by Albe *et al.*²¹. In this study, the authors took advantage of the conceptual similarities in EAM- and bond-order potentials²² and showed that covalent as well as metallic bonds can be described within the same formalism including angular terms.

The purpose of the present work is the construction of an reactive bond-order potential for the ternary W-C-H system that is able to describe the pure components as well as its binary and ternary compositions. Our strategy is to rely on a well established functional form²¹ that allows to adopt parameters for carbon and hydrocarbons from the original Brenner potential²³ and requires to derive parameters for pure tungsten and the binaries W-C and W-H. We will show that WC can be well described with this type of bond-order potential and that modelling the bcc-structure of tungsten is possible by

a straightforward extension to second-next neighbor interactions.

The approach presented here should also be applicable for modelling other bcc-metals and metal carbides.

II. METHOD

A. Bond-order formalism

The construction of an interatomic potential for the W–C–H system poses a challenge because of the widely different character of the elements and bonding types involved. Therefore, one cannot expect any analytical potential to fully describe all properties of this ternary system with equal accuracy. The bond-order potential scheme adopted in the present work, however, has been successfully applied to describe covalent^{19,23–25} and metallic bonding²¹ in different contexts. In particular, it has already been successfully applied on a metal-carbide system²¹. It is furthermore advantageous that well tested C–C, H–H, and C–H parameter sets are already available²³.

To carry out the potential construction we use an Ansatz^{21,24} which allows a systematic fitting with a minimal set of unknown parameters involved. The following equations summarize in short the functional form of the potential.

The total energy is written as a sum over individual bond energies

$$E = \sum_{i>j} f_{ij}^c(r_{ij}) \left[V_{ij}^R(r_{ij}) - \underbrace{\frac{b_{ij} + b_{ji}}{2}}_{\bar{b}_{ij}} V_{ij}^A(r_{ij}) \right]. \quad (1)$$

where the pair-like attractive and repulsive terms are taken as Morse-like pair potentials

$$\begin{aligned} V^R(r) &= \frac{D_0}{S-1} \exp\left(-\beta\sqrt{2S}(r-r_0)\right), \\ V^A(r) &= \frac{SD_0}{S-1} \exp\left(-\beta\sqrt{2/S}(r-r_0)\right), \end{aligned} \quad (2)$$

which depend on the dimer bond energy D_0 , the dimer bond distance r_0 and the adjustable parameter S . The parameter β can be determined from the ground-state oscillation frequency of the dimer. The interaction is restricted to the next neighbor sphere by a cutoff-function

$$f^c(r) = \begin{cases} 1, & r \leq R - D, \\ \frac{1}{2} - \frac{1}{2} \sin\left(\frac{\pi}{2}(r - R)/D\right), & |R - r| \leq D, \\ 0, & r \geq R + D \end{cases} \quad (3)$$

where D and R are adjustable quantities. The bond-order parameter b_{ij} includes three-body contributions and angularity

$$\begin{aligned} b_{ij} &= (1 + \chi_{ij})^{-\frac{1}{2}}, \\ \chi_{ij} &= \sum_{k(\neq i,j)} f_{ik}^c(r_{ik}) g_{ik}(\theta_{ijk}) \\ &\quad \times \omega_{ijk} \exp[2\mu_{ik}(r_{ij} - r_{ik})]. \end{aligned} \quad (4)$$

Here again the cutoff-function is included, while the indices monitor the type-dependence of the parameters, which is of importance for the description of compounds. The angular function is given by

$$g(\theta) = \gamma \left(1 + \frac{c^2}{d^2} - \frac{c^2}{d^2 + (h + \cos\theta)^2} \right). \quad (6)$$

This potential form is functionally equivalent to that used by Brenner in his hydrocarbon potential²³, except that the bond conjugation terms have been left out. We emphasize, however, that in applications where the structure and chemistry of hydrocarbon molecules is of relevance, one can and should include these terms.

If the interactions are nearest-neighbor only and only one bond type is involved, the equilibrium bonding distance r_b and the energy/bond E_b are related by the Pauling relation²¹ $E_b = -D_o \exp(-\beta\sqrt{2S}(r_b - r_o))$. In this case the relation between E_b and r_b can be conveniently illustrated as a line in a log-linear ‘‘Pauling plot’’.

Compared to the previous potentials^{19,21,24,25}, the term ω_{ijk} in (5) is new. This parameter, which depends on the types of the atoms in the triplet $i - j - k$, is necessary to make equation (4) for the bond-order compatible to the expression used in Brenner’s hydrocarbon potential which is given in equation (11) of Ref. 23. The exponential term which appears in the three-body sum of this expression

$$\exp[\alpha_{ijk}((r_{ij} - r_{0,ij}) - (r_{ik} - r_{0,ik}))] \quad (7)$$

can be rewritten as

$$\exp[\alpha_{ijk}(r_{ij} - r_{ik})] \underbrace{\exp[-\alpha_{ijk}(r_{0,ij} - r_{0,ik})]}_{\omega_{ijk}}. \quad (8)$$

By comparison with equation (5) one recognizes that our parameter $2\mu_{ik}$ corresponds to α_{ijk} and the second exponential term is a constant which we denote ω_{ijk} . In the Brenner-II parameterization²³, which is adopted in the present work for the C–C, C–H, and H–H interactions, α_{ijk} equals 4.0 \AA^{-1} except when all atoms of the triplet $i - j - k$ are C, therefore, the $2\mu_{ik}$ parameter does not need to be made dependent on all three atom types. In case that any of the three interaction atoms i, j or k is not C or H, this parameter takes the value $\omega_{ijk} \equiv 1$.

B. Fitting methodology

The underlying principles of the fitting methodology employed in the present work have been extensively described elsewhere^{21,24}. Relevant for this work is the extension on second-nearest neighbor interactions, which is described in the following:

In the body-centered cubic (bcc) structure the first and second-nearest neighbor distances differ by only 14%. Therefore, in order to avoid a very steep cutoff function, which deteriorates the quality of the potential, the cutoff is extended to

include the second-nearest neighbors. Due to this modification two different bond lengths (or equivalently bond types) have to be considered. The contributions of the two bond types can be separated, i.e. the energy of the bcc structure can be written as

$$E^{bcc} = 8 (V_{1NN}^R - b_{1NN} V_{1NN}^A) + 6 (V_{2NN}^R - b_{2NN} V_{2NN}^A),$$

where the indices 1NN and 2NN denote first and second-nearest neighbor terms, respectively. It is important to notice that the equilibrium condition ($dE/dr = 0$) does not allow to unequivocally define a *bond* energy for contribution from first and second-nearest neighbors.

If the 2μ parameter is zero, the two bond-order terms do not depend on the absolute difference, $\Delta r = r_{ik} - r_{ik}$, between the first and second nearest neighbor distance which simplifies fitting considerably (compare equation (5)). If 2μ is, however, allowed to assume nonzero values, the summation in (5) depends exponentially on Δr . Therefore, we implemented the full energy expression in our fitting routine and performed an unconstrained optimization.

Fitting the hexagonal equilibrium structure (B_h) of tungsten carbide poses a similar challenge: the cohesive energy comprises contributions from covalent W–C bonds as well as from metallic W–W bonds which is reflected by the fact that in the equilibrium structure the separation of the tungsten atoms is shorter than the second-nearest neighbor distance in bcc tungsten. This observation has two consequences: (1) since W–W interactions are present in all tungsten carbide structures, the concept of a Pauling plot cannot be applied anymore; (2) the W–W interactions must be included when fitting the W–C parameter set. In principle it is possible to fit the W–W and W–C parameter sets simultaneously. In practice, however, it has turned out advantageous to fit the W–W parameter set first and to adjust the W–C interaction subsequently with the W–W parameter set held fixed.

The parameters which we derived for the W–W, W–C, and W–H interactions are given in Table I. The table also shows the C–C, C–H, and H–H interaction parameters due to Brenner²³ but rewritten to comply with the format of the equations in Sect. II A. Brenner’s C–C parameter set is optimized with respect to molecular properties. As an alternative we have recently derived a C–C parameter set which is compatible with the present formalism¹⁹; compared to the Brenner parameter set it provides a better description of the bulk phases of carbon and, in particular, reproduces the elastic properties of diamond. Thus, depending on the intended application the one or the other C–C parameter set is to be preferred. In the following, we only consider Brenner’s parameter set as given in Table I.

III. TOTAL ENERGY CALCULATIONS

Extensive experimental data is available for the equilibrium structures of tungsten and tungsten carbide. In our fitting approach it is, however, elemental to include a variety of differently coordinated structures in order to establish the transferability of the potential. Therefore, the experimental data

needs to be complemented with results from *ab initio* calculations. While some of the required information could be obtained from literature, in some cases we had to perform calculations of our own where data was incomplete or entirely absent.

For tungsten we studied the dimer as well as the diamond (*Strukturbericht* symbol A4), simple cubic (A_h), body-centered cubic (A2) and face-centered cubic (A1) structures. In case of tungsten carbide we considered the structures of sodium chloride (B1), cesium chloride (B2), zincblende (B3), wurtzite (B4) and hexagonal tungsten carbide (B_h) as well as dimer and the trigonal ground-state structure of di-tungsten carbide (space group P3m1). Finally, for the tungsten-hydrogen system molecules of the composition WH_n with $n = 1, 2, 3, 4$, and 6 were investigated.

For tungsten and tungsten carbide we performed density-functional theory (DFT) calculations using the plane-wave pseudo-potential approach as implemented in the Castep code^{26,27}. The calculations employed the spin-polarized generalized gradient approximation as parameterized by Perdew and Wang (GGP-W91)^{28,29} and Troullier-Martins norm-conserving pseudo-potentials³⁰. We used basis set cutoff energies of 460 eV for pure tungsten and of 750 eV for the tungsten carbide phases. A Brillouin zone k -point spacing of 0.04 and the finite basis set correction²⁶ was found to converge the bcc phase calculations to better than 0.004 eV/atom. We did not perform simulations with a higher accuracy because this level was sufficient for estimating the energy difference between the phases and calculating the system geometry. For the dimer we used a k -point spacing of 0.015.

For the study of the tungsten-hydrogen molecules we used the Gaussian 98 code³¹, applying the BPW91 method^{28,29} with the 6-311++G(d,p) basis for the hydrogen atoms and SDD basis for the tungsten atoms in accordance with calculations by Wang and Andrews³².

IV. TUNGSTEN

A. Dimer and bulk properties

The fitting database for tungsten comprised experimental and first-principles data for the dimer properties, the cohesive energies and structural parameters of the diamond, simple cubic, face-centered cubic, and body-centered cubic structures as well as the elastic constants of the ground-state bcc structure. In Table II the cohesive energies, lattice parameters and elastic constants as obtained from the bond-order potential (BOP) are shown together with data from experiment and first-principles calculations. It also comprises data obtained with the analytical potential of Finnis and Sinclair³⁴ (FS) including the modifications by Ackland and Thetford⁴⁸ and the modified embedded atom method (MEAM) potential with second-nearest neighbor extension³⁵. The BOP shows the best overall agreement with the reference data. The FS potential is of comparable quality for the bulk phases but shows unrealistic dimer properties compared to experiment.

If only first-nearest neighbors were included, the BOP

TABLE I: Parameter sets for the W–C–H system. The parameter sets for W–W, W–C, and W–H have been developed in the present work. The parameter sets for C–C, C–H, H–C, and H–H due to Brenner (Ref. 23) have been rewritten to comply with the functional form used in this work. The values for ω_{ijk} are $\omega_{CCH} = 0.33946$, $\omega_{CHC} = 2.94586$, $\omega_{HHC} = 4.54415$, $\omega_{HCH} = 0.22006$ and all other $\omega = 1.0$.

parameter	W–W	W–C	W–H	C–C	H–C	C–H	H–H
D_0 (eV)	5.41861	6.64	2.748	6.0	3.6422	3.6422	4.7509
r_0 (Å)	2.34095	1.90547	1.727	1.39	1.1199	1.1199	0.74144
β (Å ⁻¹)	1.38528	1.80370	1.52328	2.1	1.9583	1.9583	1.9436
S	1.92708	2.96149	1.2489	1.22	1.69077	1.69077	2.3432
γ	1.88227×10^{-3}	7.2885×10^{-2}	5.4×10^{-3}	2.0813×10^{-4}	12.33	2.0813×10^{-4}	12.33
c	2.14969	1.10304	1.788	330.0	0.0	330.0	0.0
d	0.17126	0.33018	0.8255	3.5	1.0	3.5	1.0
h	-0.27780	0.75107	0.38912	1.0	1.0	1.0	1.0
2μ (Å ⁻¹)	0.45876	0.0	0.0	0.0	4.0	4.0	4.0
R (Å)	3.50	2.80	2.15	1.85	1.55	1.55	1.40
D (Å)	0.30	0.20	0.20	0.15	0.25	0.25	0.30

TABLE II: Comparison of properties of the dimer and various existing as well as hypothetical bulk phases of tungsten as obtained from experiment, density-functional theory (DFT) calculations, the Finnis-Sinclair (FS) potential, a modified embedded atom method (MEAM) potential, and the bond-order potential (BOP) derived in the present study. E_c : cohesive energy (eV/atom); ΔE : energy difference with respect to ground-state structure (eV/atom); r_0 : dimer bond length (Å); a : lattice parameter (Å); B : bulk modulus (GPa); B' : pressure derivative of bulk modulus; c_{ij} : elastic constants (GPa).

	Expt.	DFT		Analytical potentials		
		Ref. 33	This work	FS ^a (Ref. 34)	MEAM (Ref. 35)	BOP
dimer						
E_c	-2.5 ± 0.5^b		-2.05	-3.10		-2.71
r_0	$\sim 2.2^b$		1.95	2.52		2.34
ω	337 ^c					248
diamond (Fd$\bar{3}m$, no. 227, A4)						
ΔE			2.328	3.109	3.70	3.109
a			5.868	5.868	5.659	5.940
simple cubic (Pm$\bar{3}m$, no. 221, A_h)						
ΔE			1.217	1.501	2.61	1.614
a			2.663	2.689	2.628	2.671
face-centered cubic (Fm$\bar{3}m$, no. 225, A1)						
ΔE	0.200 ^d	0.369	0.463	0.145	0.263	0.346
a		3.960	4.084	3.927	4.013	4.005
body-centered cubic (Im$\bar{3}m$, no. 229, A2)						
E_c	-8.890		-7.406	-8.89	-8.66	-8.89
a	3.165 ^e	3.160	3.222	3.165	3.164	3.165
B	310 ^{efg} , 313 ^h	320		301	314	308
B'	4.5 ⁱ	4.20 ^j			4.79	4.9
c_{11}	522 ^e , 523 ^f , 531 ^h	552		512	533	542
c_{12}	204 ^e , 203 ^f , 204 ^h	204		196	205	191
c_{44}	161 ^e , 160 ^f , 163 ^h	149		170	163	162

^adata calculated as part of the present work.

^bReference 36.

^cReference 37.

^dCALPHAD data as cited in Reference 35.

^eReference 38, measured at room temperature.

^fReference 39, averaged values.

^g $B = (c_{11} + 2c_{12})/3$.

^hReference 40, measured at 77 K.

ⁱReference 41, measured at room temperature.

^jReference 35, DFT-GGA, us-PP.

TABLE III: Comparison of thermal, point defect and surface properties as obtained from experiment, density-functional theory (DFT) calculations, a modified embedded atom method (MEAM) potential (Ref. 35), and the bond-order potential (BOP) derived in the present study. T_m : melting point (K); ΔH_f : enthalpy of fusion at the melting point (kJ/mole); $\Delta V/V_s$: volume change upon melting (%); ρ_l : density of the liquid at the melting point (g/cm^3); α : coefficient of linear thermal expansion ($10^{-6}/\text{K}$); H_v^f , H_i^f : vacancy and interstitial formation enthalpies (eV); ΔV_v , ΔV_i : vacancy and interstitial formation volumes in units of the atomic volume; $\gamma^{(100)}$: surface energy for (100) surface (J/m^2); $\Delta_{ij}^{(hkl)}$: spacing between layers i and j of (hkl) surface (%); $\Delta a_{12}^{(211)}$: lateral shift between first and second layer for the (211) surface reconstruction (\AA).

	Expt.	Analytical potentials	
		MEAM	BOP
T_m	3695 ^a	4600	2750 \pm 50
ΔH_f	52.3 ^a	33.0	27.4
$\Delta V/V_s$		3.2	4.3
ρ_l	17.6 ^a		17.1
α_L	4.5 ^b		6.6
H_v^f	3.6 \pm 0.2 ^c	3.95	1.68
ΔV_v			-0.32
H_i^f		8.98	8.31
ΔV_i			1.95
$\gamma^{(100)}$	3.220 ^d		1.446
$\Delta_{12}^{(100)}$	-4 - -8 ^d		-8.4
$\Delta_{23}^{(100)}$	+0.5 \pm 0.5 ^d		-0.9
$\Delta_{12}^{(110)}$	-3.1 \pm 0.6 ^e		-3.9
$\Delta_{23}^{(110)}$	0.0 \pm 0.6 ^e		+0.1
$\Delta_{34}^{(110)}$	0.0 \pm 1.0 ^e		0.0
$\Delta_{12}^{(211)}$	-12.4 ^f , -9.3 ^g		-12.0
$\Delta a_{12}^{(211)}$	-0.09 ^f , -0.10 ^g		-0.08

^aReference 38.

^bReference 42.

^cReference 43.

^dReference 44.

^eReference 45.

^fReference 46.

^gReference 47.

would fulfill the Pauling relation exactly as indicated by the dashed line in the upper panel of Fig. 1. In that case, the data points for the simple cubic and bcc phases obviously deviate quite significantly. However, by including the second nearest neighbor shells of these structures it is possible to capture the observed upward bending (Fig. 1). This modification guarantees the good agreement of the BOP with the reference data.

The lower panel of Fig. 1 provides a graphical comparison of the performance of the different potentials. It underlines the good agreement of the BOP and the FS potential with the reference data and shows the MEAM potential to underestimate the cohesion in lower-coordinated structures such as diamond and simple cubic.

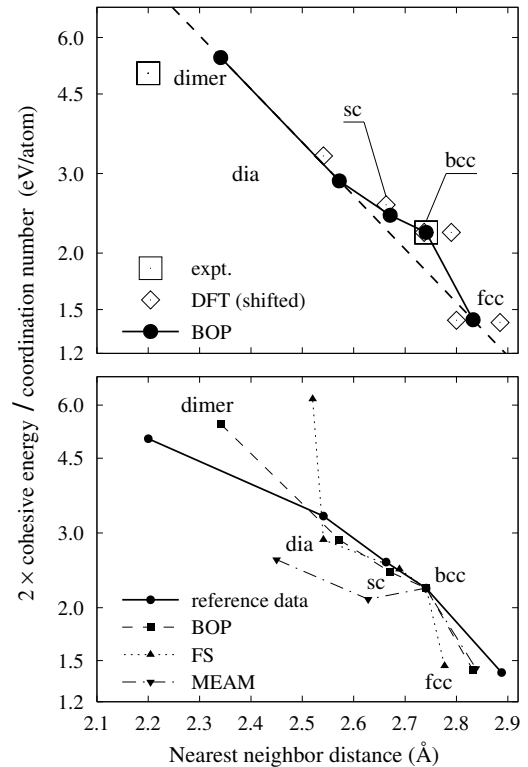


FIG. 1: Dependence between the cohesive energy normalized by the coordination number on the nearest neighbor distance. If only nearest neighbors were considered the regular Pauling plot would be obtained which predicts a logarithmic dependence between bond energy and length as indicated by the dashed line in the upper panel. The cohesive energies and bond lengths obtained from density-functional theory (DFT) calculations are shifted and rescaled, respectively such that the data for the ground-state structure reproduces the experimental values. The lower panel compares three different potentials with respect to their ability to reproduce the reference data.

B. Thermal and point defect properties

In order to determine the melting point of tungsten at ambient pressure, we performed molecular dynamics simulations of a solid-liquid interface⁴⁹. The simulation cell comprised 2960 atoms, temperature and pressure was controlled using the Berendsen thermostat and barostat⁵⁰, and the samples were equilibrated for up to 0.5 ns. For temperatures above 2800 K complete melting is observed, while for temperatures below 2700 K the crystalline phase grows, leading to an estimate for the melting point of 2750 \pm 50 K.

From the temperature dependence of potential energy and cell volume we determined the enthalpy of fusion at the melting point, the density change upon melting and an estimate for the coefficient of linear thermal expansion. The results of this analysis are included in Table III revealing acceptable agreement with experiment.

Table III also summarizes the formation enthalpies and volumes for the vacancy and the interstitial in tungsten as calculated using the BOP and compares them to data from experiment and other analytical potentials. The vacancy formation

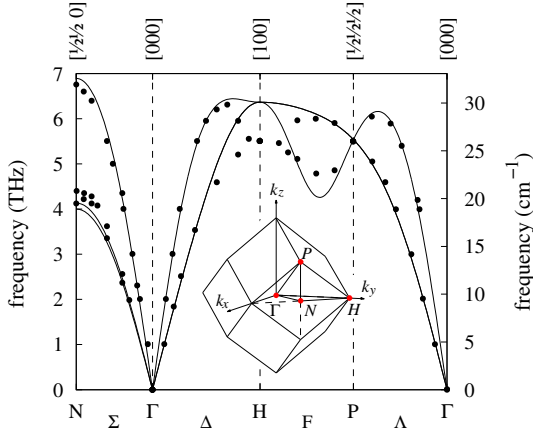


FIG. 2: Phonon dispersion curves obtained using the BOP derived in this work. Experimental data points are indicated by black dots (Ref. 52).

enthalpy is clearly too low compared to experiments. Within the present scheme this deficiency is closely related to the cohesive energy and the elastic properties and, therefore, cannot be corrected without sacrificing other important properties. The observed interstitial configuration is the [110]-dumbbell in agreement with other analytical potentials.

C. Surfaces

Surface energies and changes in interlayer spacing were calculated for the (100), (110) and (211) surfaces of bcc tungsten, which have been extensively studied experimentally and theoretically^{44–47,51}. First we examined whether surface reconstruction occurs on these surfaces by performing high-temperature (300 – 2000 K) annealing and subsequent cooling. For the (100) surface we also manually generated the experimentally observed $\sqrt{2} \times \sqrt{2}R45^\circ$ reconstruction and subsequently relaxed it. In this reconstruction the top layer atoms are shifted by about 0.237 \AA forming a zigzag pattern⁴⁴. We found that in our model the (100) surface does not reconstruct laterally, while on the (211) surface the top atom rows are shifted laterally by $\Delta a_{12} = -0.08 \text{ \AA}$ in the [111] direction, in excellent agreement with the experimental values of -0.10 \AA ⁴⁷ and -0.09 \AA ⁴⁶. The lattice plane relaxations and surface energy are compiled in Table III for those cases where experimental data is available. The structural parameters compare well with experiment, while the surface energy is about a factor of two too small.

D. Phonon dispersion

As a final test we derived the phonon dispersion for bcc tungsten by diagonalization the dynamical matrix at different k -points⁵³. The result is shown in Fig. 2 together with data points from experiment⁵². The phonon frequency at the

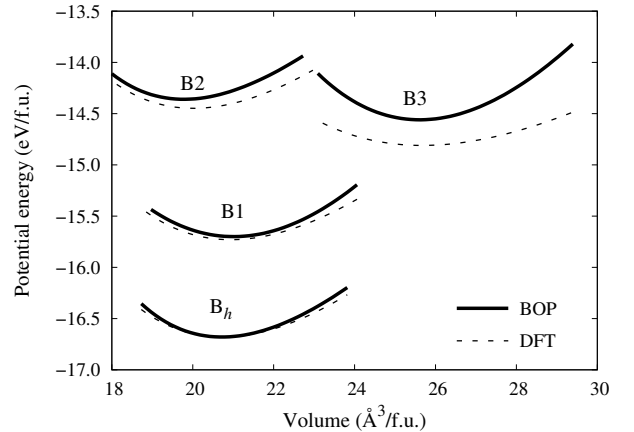


FIG. 3: Energy-volume curves at zero Kelvin as obtained with the bond-order potential (BOP) in comparison with data from density-functional theory (DFT) calculations. The cohesive energies and lattice constants calculated via DFT have been shifted and scaled, respectively, to comply with the experimental data for the ground state (B_h) structure.

H-point is somewhat overestimated but otherwise the agreement with experiment is excellent including the splitting of the transverse phonon branches at the N-point.

V. TUNGSTEN CARBIDE

A. Dimer and bulk properties

The ground-state or tungsten carbide is a hexagonal structure with space group symmetry $P\bar{6}m2$. It can be visualized as a hexagonal-closed packed lattice with layers of alternating atom types along the c -axis⁵⁴. The fitting database comprised the cohesive energy and the lattice parameters of the ground-state structure along with the full set of elastic constants. It also included the dimer energy as well the cohesive energies and lattice parameters of several stoichiometric, hypothetical structures. The resulting properties are compiled in Table IV which shows a very good agreement between the reference data and the BOP. The excellent description of the coordination dependence of energy and volume is further illustrated in Fig. 3 which shows the energy-volume curves as obtained from the BOP in comparison with data from DFT calculations.

As a test of the potential we determined the properties of the rhombohedral W_2C phase which has space group symmetry $P3m1$ ⁴². The BOP successfully reproduces the symmetry of the structure with lattice constants of $a = 2.984 \text{ \AA}$ and $c = 5.037 \text{ \AA}$ (at 0 K) in good agreement with values calculated via DFT of $a = 3.127 \text{ \AA}$ and $c = 4.741 \text{ \AA}$ (at 0 K), and experimental values of $a = 3.001 \text{ \AA}$ and $c = 4.774 \text{ \AA}$. The DFT calculation yields a cohesive energy of $E_c = -7.27 \text{ eV/atom}$. It is well known that the cohesive energies obtained via DFT calculations are subject to systematic errors while the energy differences are typically reliable. This trend is also observed for the other structures considered in this study. In order to correct

TABLE IV: Comparison of properties of the dimer and several existing and hypothetical bulk structures of tungsten-carbide as obtained from experiment, *ab initio* calculations, density-functional theory (DFT) calculations, and from the bond-order potential developed in this work (BOP). Symbols as in Table II unless otherwise noted. E_c : cohesive energy per formula unit (eV/f.u.); ΔE : energy difference with respect to ground-state structure (eV/f.u.); c/a : axial ratio of hexagonal tungsten carbide; V : volume ($\text{\AA}^3/\text{f.u.}$); $\alpha_L^{a,c}$: coefficient of linear thermal expansion along the a and c -axes ($10^{-6}/\text{K}$).

	Expt.	<i>Ab initio</i>	DFT	BOP
dimer				
E_c		-6.14 ^a	-4.73, -6.64 ^b	-6.64
r_0	1.713 ^c	1.759 ^a	1.75	1.905
ω	983 ^c	928 ^a		1021
zincblende (F$\bar{4}3m$, no. 216, B3)				
ΔE			1.87	2.12
a			4.801	4.679
B			246	511
wurtzite (P6$_3$mc, no. 186, B4)				
ΔE			1.83	1.01
a			3.184	2.828
c/a			1.928	1.822
rocksalt (Fm$\bar{3}m$, no. 225, B1)				
ΔE			0.95	0.98
a			4.482	4.380
B			346	405
cesium chloride (Pm$\bar{3}m$, no. 221, B2)				
ΔE			2.32	2.32
a			2.779	2.704
B			350	411
tungsten carbide (P$\bar{6}m2$, no. 187, B$_h$)				
E_c	-16.68 ^d		-15.01	-16.68
a	2.907 ^e		2.979	2.917
c/a	0.976 ^e		0.975	0.964
V	20.74		22.32	20.72
B	443 ^f		368	443
B'			4.2	5.1
c_{11}	720 ^g		651	710
c_{33}	972 ^g		887	896
c_{12}	254 ^g		183	224
c_{13}	267 ^g		189	305
c_{44}	328 ^g			267
c_{66}	233 ^g		234	243
T_m	3049 ^h , 3143 ^e			3050 \pm 50
ΔH_m				123
$\Delta V/V_s$				16.4
ρ_l				12.9
α_L^a	5.2 ^e			5.0
α_L^c	7.3 ^e			5.2

^aReference 55.

^bshifted such that B $_h$ ground state structure agrees with experiment.

^cReference 56.

^dReference 38

^eReference 42

$${}^f B = \frac{2}{9}(c_{11} + c_{12} + 2c_{13} + \frac{1}{2}c_{33})$$

^gReference 57

^hReference 58.

for this deficiency, as a first approximation one can interpolate between the offsets obtained for W, WC, and C obtained with the same method which gives $E_c = -8.43$ eV/atom. This value can be used for benchmarking the BOP; the latter predicts a cohesive energy of $E_c = -8.00$ eV/atom in very good agreement with the interpolated value. The good agreement of the structural parameters as well as the cohesive energy shows the ability of the BOP to describe structures which are quite different from the ones considered during fitting.

B. Thermal properties

In order to assess the thermodynamic data of tungsten-carbide we adopted the same approach as in Sect. V B. In this case the simulation cell contained 3240 atoms and was equilibrated for up to 0.5 ns. From these simulations we obtained an estimate for the melting point of 3050 ± 50 K which agrees very well with the experimental value of 3049 K⁵⁸.

In addition we performed molecular dynamics simulations of the isolated phases. Crystalline as well as molten cells containing 784 and 1620 atoms, respectively, were equilibrated for up to 0.2 ns at temperatures between 100 and 3500 K (crystalline phase) and 2500 and 4500 K (molten phase). From these runs a number of thermal properties were determined which are compiled in Table IV. Overall the agreement with the reference data is good.

C. Point defects

Only limited information is available on point defects in hexagonal tungsten carbide. Rempel *et al.* performed positron annihilation spectroscopy experiments⁵⁹. While they identified tungsten as well as carbon vacancies, they found the latter to be formed preferentially.

We calculated the formation enthalpies and volumes for several point defect configurations in tungsten carbide using the thermodynamics formalism due to Quiang *et al.*⁶⁰ adapted for point defects by Zhang and Northrup⁶¹. In the following formation enthalpies are reported for an average chemical potential ($\Delta\mu = 0$ in equation (2) of Ref. 61). The BOP gives formation enthalpies of 3.4 and 0.7 eV for the tungsten and carbon vacancies, respectively; the carbon interstitial has a formation enthalpy of 2.7 eV and the tungsten interstitial is energetically highly unfavorable with a formation enthalpy of 12.3 eV. Thereby, the BOP correctly reproduces the experimental observation that carbon vacancies are energetically more favorable than tungsten vacancies. Within our model the formation of a carbon vacancy requires the breakage of six W-C bonds; in order to form a tungsten vacancy also eight metallic W-W bonds need to be broken, which readily explains the extent of the observed asymmetry in the formation enthalpies.

For both interstitials the BOP predicts ground-states in which the surplus atom is located in the carbon plane in one of the channels along the [0001] axis as illustrated for the carbon

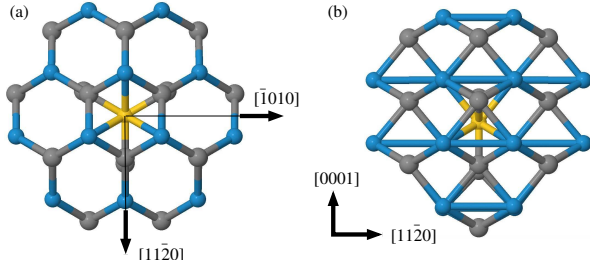


FIG. 4: Carbon interstitial configuration in hexagonal tungsten carbide viewed along the (a) $[0001]$ and (b) $[2\bar{1}\bar{1}0]$ directions.

interstitial in Fig. 4. The lattice relaxation in the vicinity of the defect is comparable in both cases.

D. Surfaces

Surface energies were calculated for the relaxed but unreconstructed (0001) , $(1\bar{1}00)$, and $(2\bar{1}\bar{1}0)$ faces. For the (0001) surface carbon as well as tungsten termination was considered, and for the $(1\bar{1}00)$ surface we considered the two types of termination described in Ref. 63. The method employed to evaluate the surface energies is explained in Appendix A. The resulting values together with the interlayer relaxation are given in Table V in comparison with data from DFT calculations. The agreement of the structural parameters is good and although the surface energies are consistently underestimated, their ordering is correctly reproduced. Analogous to the case of the vacancies the asymmetry between the C and W terminated surfaces is captured by the BOP in a physically correct manner, since it takes into account the contributions of the covalent W–C bonds as well as the contributions of the metallic W–W bonds.

VI. TUNGSTEN-HYDROGEN

Tungsten does not form a bulk hydride but hydrogen is endothermally soluble in W with an enthalpy of solution of 1.04 ± 0.17 eV (Ref. 64). Furthermore, several tungsten-hydrogen molecules have been experimentally observed, and their properties have been studied with Hartree-Fock methods^{32,65–69}. However, except for the dimer these are only weakly bound. Hence we chose to fit our potential to the WH molecules with emphasis on the dimer. After the systematic fitting we then manually adjusted the parameters S , γ as well as the cutoff range to get the solubility energy of H in bulk W approximately right while ensuring that the H impurities occupy tetrahedral interstitial sites as observed experimentally⁷⁰. Finally, the remaining parameters were fitted to a set of properties of small WH_n ($n \leq 4$) molecules.

The properties of various small molecules as obtained using the BOP are compared in Table VI with *ab initio* data revealing good overall agreement. The ground-state oscillation frequencies agree well with experimental data³². No effort was made to describe the true ground-state structure of WH_6

TABLE V: Surface energies and relaxations of unreconstructed WC-surfaces as calculated with the bond-order potential (BOP) developed in this work in comparison with data from density-functional theory (DFT) calculations (Refs. 62,63). For non-stoichiometric surfaces the surface energy is given for an intermediate chemical potential ($\Delta\mu = 0$ in equation (A1)). Symbols as in Table III.

	DFT	BOP
(0001)-C surface		
γ_s	6.0	6.05
Δ_{12}	–22.5	–10.4
Δ_{23}	+5.6	–0.5
Δ_{34}	–2.1	+0.4
Δ_{45}	+0.7	+0.1
(0001)-W surface		
γ_s	3.6	2.90
Δ_{12}	–4.2	–3.8
Δ_{23}	+2.1	+1.5
Δ_{34}	0.0	+0.3
Δ_{45}	+0.7	+0.3
$(1\bar{1}00)$-C – type I surface		
γ_s	4.6	2.87 ^a , 3.01 ^b
Δ_{12}	~ -20	–15.4
Δ_{23}	^c	–0.7
$(1\bar{1}00)$-W – type I surface		
γ_s	2.7	1.72 ^a , 1.58 ^b
Δ_{12}	^c	–4.7
$(1\bar{1}00)$-C – type II surface		
γ_s	8.7	6.47 ^a , 6.79 ^b
Δ_{12}	~ -20	–10.3
Δ_{23}	^c	–1.1
$(1\bar{1}00)$-W – type II surface		
γ_s	5.2	3.87 ^a , 3.56 ^b
$(2\bar{1}\bar{1}0)$ surface		
γ_s		2.79
Δ_{12}		–5.4

^a $\alpha = 1.67$ where α is the ratio of the surface energies of C and W terminated $(1\bar{1}00)$ surfaces (see Sect. A).

^b $\alpha = 1.91$.

^cIn Ref. 63 all relaxations except for the first inter-planar spacing (Δ_{12}) of C terminated surfaces were found to be at least one order of magnitude smaller than the latter.

due its complex structure and several alternative geometries very close in energy^{32,68,69}. The BOP gives a ground-state with D_{3h} symmetry the cohesive energy and bond lengths of which are very similar to the results of quantum-mechanical calculations.

As an additional test, we considered the reconstruction of the hydrogenated (110) surface of tungsten ((1×1) -H W (110) surface) described in Ref. 45. The structural parameters of this reconstruction are summarized and compared to data from experiment and density-functional theory (DFT) calculations in Table VII. The overall agreement is good and our model successfully reproduces the fundamental features of the reconstruction.

TABLE VI: Comparison of properties of several WH_n molecules as obtained from *ab initio* calculations, experiments, density functional theory (DFT) calculations, and the bond-order potential (BOP) developed in the present work. E_c : cohesive energy (eV/atom); r_0, r'_0 : bond lengths (Å); θ, θ' : H-W-H bond angles (deg); ω : ground-state oscillation frequency of W-H bond (cm^{-1}).

	<i>Ab initio</i>	Expt. Ref. 32	DFT		BOP
			Ref. 32	This work	
WH					
E_c	-1.345 ^a			-1.374	-1.374
r_0	1.727 ^a	1.727	1.715	1.714	1.727
ω	1897 ^a	1860	1915		1860
WH₂ (C₂)					
E_c				-1.851	-1.820
r_0	1.73 ^b		1.717	1.717	1.730
θ	117.2 ^b		112.9	112.9	112.9
ω		1832	1928		1852
WH₃ (C_{3v})					
E_c				-2.112	-2.033
r_0	1.689 ^c		1.716	1.716	1.733
θ	112.8 ^c		112.8	112.6	112.9
ω		1895	1946		1846
WH₄ (T_d)					
E_c				-1.937	-2.154
r_0			1.712	1.715	1.736
θ			109.5	109.5	109.5
ω		1921	1983		1840
WH₆ (C_{3v}, BOP: D_{3h})					
E_c				-2.417	-2.220
r_0	1.728 ^d		1.715	1.715	1.754
r'_0	1.656 ^d		1.674	1.674	
θ	116.1 ^d		114.7	114.7	98.5
θ'	61.2 ^d		62.4	62.4	

^aReference 65

^bReference 66

^cReference 67

^dReference 69

TABLE VII: Comparison of structural parameters of the reconstructed (1 × 1)-H W(110) surface as obtained from experiment, density-functional theory (DFT) calculations (both from Ref. 45) and using the bond order potential (BOP). Symbols as in Table III unless otherwise noted. d_H : separation between hydrogen top-layer and the first tungsten layer (Å), y_H : lateral relaxation of hydrogen atoms (Å), y_1 : lateral relaxation of first tungsten layer (Å). Consult Ref. 45 for the exact definitions of the parameters.

	Expt.	DFT	BOP
Δ_{12}	-1.7 ± 0.6	-1.4	-3.2
Δ_{23}	0.0 ± 0.9	-0.3	+0.1
Δ_{34}	0.0 ± 0.9	-0.1	0.0
y_1	0.0 ± 0.1	0.0	0.0
d_H	1.20 ± 0.25	1.09	1.05
y_H	0.56 ± 0.36	0.67	0.20

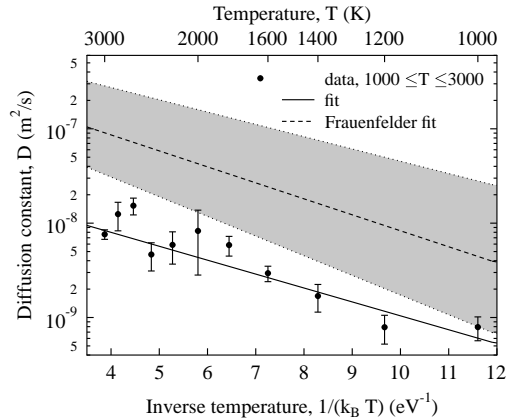


FIG. 5: Diffusion data and Arrhenius fit obtained from molecular dynamics simulations using the BOP developed in the present work in comparison with Arrhenius fit to experimental data (Ref. 64). The shaded area indicate the uncertainty region for the experimentally obtained diffusion parameters.

Finally, we also derived the diffusivity of H in W. To this end, molecular dynamics simulations were carried out. The simulation box was approximately cubic with a side length of about 38 Å and contained a single hydrogen atom equivalent to a concentration of 0.03%. The temperature of the system was varied between 1000 and 3000 K using the Berendsen thermostat and the Berendsen barostat was employed to maintain a pressure of about 0 kbar. The results of the simulations are plotted in Fig. 5. The data points can be fitted by an Arrhenius law ($D = D_0 \exp[-E_A/k_B T]$) with $D_0 = (3.1 \pm 0.6) \times 10^{-8} \text{ m s}^{-2}$ and $E_A = 0.34 \pm 0.03 \text{ eV}$. The result of the Arrhenius fit is also shown in Fig. 5 together with the fit to experimental data by Frauenfelder⁶⁴ ($D_0 = 4.1^{+5.0}_{-2.0} \times 10^{-7} \text{ m s}^{-2}$, $E_A = 0.39 \pm 0.09 \text{ eV}$). Thus the activation energy for migration obtained with our model compares very well with experiment; the prefactor deviates from the experimental value, but the agreement is still fair considering the large uncertainty in the experimental data.

VII. CONCLUSIONS

The well established bond-order potential (BOP) scheme has been extended to include second neighbors interactions for pure elements (W) as well as compounds (WC). Thereby it is possible to (1) capture the deviation from the Pauling relation observed for the simple and body-centered cubic (bcc) structures of tungsten, and (2) to include realistically the contributions of covalent (W-C) as well as metallic (W-W) bonds in tungsten carbide.

The extended BOP scheme has been applied to develop potentials for the W-C-H system. The W potential provides a good description of the coordination dependence of structural parameters and cohesive energies. Thermal, point defects as well as surface properties are reasonably described. Overall, the performance of the W bond-order potential is comparable

to Finnis-Sinclair^{34,48} and modified embedded atom method potentials³⁵.

The structural and elastic properties obtained with the WC potential compare well with experiment and density-functional theory calculations. It also yields reasonable agreement with the available reference data for thermal and point defects properties. It has been, furthermore, shown to be capable of reproducing energies and relaxation of several unreconstructed surfaces. The W–H potential correctly describes the solubility of H in bcc W and yields good agreement with experimental data on diffusion. It also successfully reproduces the energetics and structures of small WH_n molecules. For the C–C, C–H, and H–H interactions the well tested parameterizations due to Brenner²³ is used. It has been rewritten to comply with the functional form employed in present work which should considerably simplify implementation of the BOP into existing Tersoff routines. Alternatively, the C–C parameter set of Ref. 19 can be employed which is advantageous if the bulk properties of carbon are of interest.

The potentials developed in the present work provide a realistic description of the material over a wide range of coordinations. They are expected to be applicable for simulations of a variety of processes and phenomena in the W–C–H system involving bulk material as well as surfaces. In particular, they are suitable for modeling surface erosion at WC surfaces which is of interest in the context of the deterioration and decomposition of W and WC parts in current and future fusion reactors. Work in this directions is currently underway. Repulsive potentials required to realistically describe the close ion-ion encounters during high-energy collisions are provided in the appendix.

Acknowledgments

The research was supported by Association EURATOM/TEKES under the FUSION programme. This joint study was made possible by the support of the Academy of Finland (project No. 204461) and the German foreign exchange service (DAAD) through a bilateral travel program, and was also partly supported by Academy of Finland under project No. 205729. Grants of computer time from the Center for Scientific Computing in Espoo, Finland are gratefully acknowledged.

APPENDIX A: CALCULATION OF SURFACE ENERGIES

The surface energies of non-stoichiometric surfaces depend on the chemical potential according to⁶⁰

$$\begin{aligned} \gamma_s = & \left(E_{slab} - \frac{1}{2}(n_W + n_C)\mu_{WC}^{bulk} \right. \\ & - \frac{1}{2}(n_W - n_C)(\mu_W^{bulk} - \mu_C^{bulk}) \\ & \left. - \frac{1}{2}(n_W - n_C)\Delta\mu \right) / 2A \end{aligned} \quad (A1)$$

where E_{slab} is the total energy of the surface slab, n_W and n_C are the numbers of tungsten and carbon atoms respectively, A is the cross sectional area, and μ_i^{bulk} denotes the chemical potential of phase i in its respective standard state. The variation of the surface energy with chemical potential is expressed by the last term which is subject to the constraint $\Delta H_f^{WC} \leq \Delta\mu \leq -\Delta H_f^{W_2C}$ where ΔH_f^i is the formation enthalpy of phase i (Ref. 62). Using equation (A1) one can directly calculate the surface energies for the (0001) and (2 $\bar{1}$ 10) surfaces.

The situation is more involved for the (1 $\bar{1}$ 00) surface for which each termination (C, W) can occur in two different types as discussed in Ref. 63. Therefore, in any slab geometry two different surfaces are present. If stoichiometry is required, the possible combinations are (1 $\bar{1}$ 00)-C-I + (1 $\bar{1}$ 00)-W-I (setup A) and (1 $\bar{1}$ 00)-C-II + (1 $\bar{1}$ 00)-W-II (setup B). The authors of Ref. 63 used these two setups to compute the *sums* of the respective surface energies. They then separated the individual contributions by assuming the ratio, α , between the surface energies of the carbon and tungsten terminated surfaces to be the same as for the (0001) surfaces for which they took the data from Ref. 62 assuming $\Delta\mu = 0$. In the following we demonstrate that within the same approximation by using one additional geometry one can derive the ratio α from calculations for (1 $\bar{1}$ 00) surfaces only.

In addition to the two geometries mentioned above one can construct non-stoichiometric slabs with pure C or W terminations for which one side of the slab is of type I (setup C) and the other one of type II (setup D). Using (A1) one can again compute the respective surface energies. Thus, we obtain four different sums of surface energies the relation between which can be expressed by a set of linear equations

$$\begin{pmatrix} 1 & 1 & 0 & 0 \\ 0 & 0 & 1 & 1 \\ 1 & 0 & 1 & 0 \\ 0 & 1 & 0 & 1 \end{pmatrix} \cdot \begin{pmatrix} \gamma_s^{(1\bar{1}00)-C-I} \\ \gamma_s^{(1\bar{1}00)-W-I} \\ \gamma_s^{(1\bar{1}00)-C-II} \\ \gamma_s^{(1\bar{1}00)-W-II} \end{pmatrix} = \begin{pmatrix} \gamma_A \\ \gamma_B \\ \gamma_C \\ \gamma_D \end{pmatrix} \quad (A2)$$

where γ_s^i denotes the surface energy of surface i and γ_j the sum of surface energies obtained for setup j . Since this set of equations is linearly dependent one additional constraint is required. (One can also exploit the relation between the sums to check the fidelity of a set of calculations since $\gamma_A + \gamma_B = \gamma_C + \gamma_D$). Following the discussion above one can assume $\gamma_s^{(1\bar{1}00)-C-I} / \gamma_s^{(1\bar{1}00)-W-I} \equiv \gamma_s^{(1\bar{1}00)-C-II} / \gamma_s^{(1\bar{1}00)-W-II} \equiv \alpha$. Then equation (A2) can be easily solved yielding an expression for α in terms of γ_A , γ_B , and γ_C

$$\alpha = \frac{\gamma_C}{\gamma_A + \gamma_B + \gamma_C}$$

and the individual surface energies can be computed from the following relations

$$\begin{aligned} \gamma_s^{(1\bar{1}00)-C-I} &= \gamma_C / (1 + \gamma_B / \gamma_A) \\ \gamma_s^{(1\bar{1}00)-W-I} &= \gamma_s^{(1\bar{1}00)-C-I} / \alpha \\ \gamma_s^{(1\bar{1}00)-C-II} &= \gamma_C / (1 + \gamma_A / \gamma_B) \\ \gamma_s^{(1\bar{1}00)-W-II} &= \gamma_s^{(1\bar{1}00)-C-II} / \alpha. \end{aligned}$$

Using the values for γ_i calculated with the BOP and setting $\Delta\mu = 0$ we obtain a ratio of $\alpha = 1.91$ to be compared with a value of $\alpha = 1.67$ derived from the data in Ref. 62 and a value of $\alpha = 2.09$ obtained from the BOP data for the (0001) surface. In Table V the surface energies are given for $\alpha = 1.67$ and $\alpha = 1.91$ which shows the small difference to be sufficient to change the energetic ordering of the surfaces. (For $\alpha = 2.09$ the values vary slightly from the case $\alpha = 1.91$ but the energetic ordering remains unaltered).

In summary, we have shown that one can obtain a consistent set of individual surface energies for the (1100) face without invoking data for surfaces of a different orientation. The results indicate that the energetic ordering of the various surfaces can depend quite sensitively on the ratio α .

APPENDIX B: MODIFICATION OF THE REPULSIVE POTENTIAL

In applications for which high-energetic ($E_{kin} \gg 10$ eV) collisions between atoms need to be taken into account, it is necessary to modify the repulsive part of the potential.

To this end, we first derive an accurate repulsive pair potential V^{DFT} for a dimer employing a density-functional theory method⁷¹. We then construct a modified repulsive potential,

V_{mod}^R , using

$$V_{mod}^R(r) = V^{DFT}(r)[1 - F(r)] + V^R(r)F(r).$$

where V^R is the potential for states close to equilibrium described in the main text, and the Fermi function

$$F(r) = \frac{1}{1 + \exp[-b_f(r - r_f)]}.$$

The value of the constants b_f and r_f are chosen such that the potential is essentially unmodified at the equilibrium and longer bonding distances, and that a smooth fit at short separations with no spurious minima is achieved for all realistic coordination numbers. Using this approach we obtained the parameters given in Table VIII. These same values also give smooth fits to the Ziegler-Biersack-Littmark universal repulsive potential⁷².

TABLE VIII: Parameters for repulsive potentials.

	W-W	W-C	W-H	C-C	C-H	H-H
r_f (Å)	1.3	1.2	0.5	0.6	0.5	0.35
b_f (1/Å)	12	7	7	8	10	15

- ¹ International Tungsten Industry Association (ITIA), <http://www.itia.org.uk/>.
- ² J. P. Hirvonen, J. Koskinen, A. Anttila, D. Stone, and C. Paszkiet, *Mater. Sci. Eng.* **90**, 343 (1987).
- ³ D. R. McIntyre, G. T. Burstein, and A. Vosen, *J. Power Sources* **107**, 67 (2002).
- ⁴ A. Mobius and K. Wiesener, *Ber. Bunsenges. Phys. Chem. Chem. Phys.* **94**, 1039 (1990).
- ⁵ J. D. Fitzgerald, Y. Chen, and M. J. Conway, *Appl. Phys. A* **A76**, 107 (2003).
- ⁶ ITER Physics Basis Editors, ITER Physics Expert Group Chairs and Co-Chairs and ITER Joint Central Team and Physics Integration Unit, *Nuclear Fusion* **39**, 2137 (1999).
- ⁷ J. Küppers, *Surf. Sci. Rep.* **22**, 249 (1995).
- ⁸ E. Salonen, K. Nordlund, J. Keinonen, and C. H. Wu, *Phys. Rev. B* **63**, 195415 (2001).
- ⁹ W. M. Wang, J. Roth, S. Lindig, and C. H. Wu, *J. Nucl. Mater.* **299**, 124 (2001).
- ¹⁰ D. P. Coster, X. Bonnin, B. Braams, D. Reiter, R. Schneider, and the ASDEX Upgrade Team, *Physica Scripta* **T108**, 7 (2004).
- ¹¹ M. S. Daw and M. I. Baskes, *Phys. Rev. B* **29**, 6443 (1984).
- ¹² M. Finnis and J. Sinclair, *Phil. Mag. A* **50**, 45 (1984).
- ¹³ J. Moriarty, *Phys. Rev. B* **42**, 1609 (1990).
- ¹⁴ A. Carlsson, *Phys. Rev. B* **44**, 6590 (1991).
- ¹⁵ W. Xu and J. B. Adams, *Surface Science* **301**, 371 (1994).
- ¹⁶ J. Tersoff, *Phys. Rev. B* **39**, 5566 (1989).
- ¹⁷ H. Huang, N. Ghoniem, and J. Wong, *Mod. Simul. Mater. Sci. Eng.* **3**, 615 (1995).
- ¹⁸ R. Devanathan, T. D. de la Rubia, and W. Weber, *J. Nucl. Mater.* **253**, 47 (1998).
- ¹⁹ P. Erhart and K. Albe, *Phys. Rev. B* **71**, 035211 (2005).
- ²⁰ J. Li, D. Liao, S. Yip, R. Najafabadi, and L. Ecker, *J. Appl. Phys.* **93**, 9072 (2003).
- ²¹ K. A. Albe, K. Nordlund, and R. S. Averback, *Phys. Rev. B* **65**, 195124 (2002).
- ²² D. W. Brenner, *Phys. Rev. Lett.* **63**, 1022 (1989).
- ²³ D. W. Brenner, *Phys. Rev. B* **42**, 9458 (1990), *ibid.* **46**, 1948 (1992).
- ²⁴ K. Albe, K. Nordlund, J. Nord, and A. Kuronen, *Phys. Rev. B* **66**, 035205 (2002).
- ²⁵ J. Nord, K. Albe, P. Erhart, and K. Nordlund, *J. Phys.: Condens. Matter* **15**, 5649 (2003).
- ²⁶ *CASTEP Users Guide* (Accelrys Inc., San Diego, CA, 2001).
- ²⁷ V. Milman, B. Winkler, J. A. White, C. J. Pickard, M. C. Payne, E. V. Akhmatkaya, and R. H. Nobes, *Int. J. Quant. Chem.* **77**, 895 (2000).
- ²⁸ A. D. Becke, *Phys. Rev. A* **38**, 3098 (1988).
- ²⁹ J. P. Perdew and Y. Wang, *Phys. Rev. B* **45**, 13244 (1992).
- ³⁰ N. Troullier and J. L. Martins, *Phys. Rev. B* **43**, 1993 (1991).
- ³¹ M. J. Frisch, G. W. Trucks, H. B. Schlegel, G. E. Scuseria, M. A. Robb, J. R. Cheeseman, V. G. Zakrzewski, J. A. Montgomery, Jr., R. E. Stratmann, J. C. Burant, et al., *Gaussian 98 (Revision A.11)* (Gaussian Inc., Pittsburgh, PA, 2001).
- ³² X. Wang and L. Andrews, *J. Phys. Chem. A* **106**, 6720 (2002).
- ³³ K. Einarsson, B. Sadigh, G. Grimvall, and V. Ozolins, *Phys. Rev. Lett.* **79**, 2073 (1997).
- ³⁴ M. W. Finnis and J. E. Sinclair, *Phil. Mag. A* **50**, 45 (1984).
- ³⁵ B.-J. Lee, M. I. Baskes, H. Kim, and Y. K. Cho, *Phys. Rev. B* **64**, 184102 (2001).
- ³⁶ M. D. Morse, *Chem. Rev.* **86**, 1049 (1986).
- ³⁷ J. R. Lombardi and B. Davis, *Chem. Rev.* **102**, 2431 (2002).
- ³⁸ D. R. Lide, ed., *CRC Handbook of Chemistry and Physics* (CRC Press, Boca Raton, 2004), 85th ed.
- ³⁹ A. Every and A. McCurdy, *Landolt-Börnstein: numerical data*

- and functional relationships in science and technology, *New Series*, vol. III/29A (Springer, Heidelberg, 1992).
- ⁴⁰ D. I. Bolef and J. de Klerk, *J. Appl. Phys.* **33**, 2311 (1962).
- ⁴¹ J. H. Rose, J. R. Smith, F. Guinea, and J. Ferrante, *Phys. Rev. B* **29**, 2963 (1984).
- ⁴² H. O. Pierson, *Handbook of refractory carbides and nitrides: properties characteristics, processing, and applications* (Noyes Publications, Westwood, NJ, 1996).
- ⁴³ P. Ehrhart, *Landolt-Börnstein: numerical data and functional relationships in science and technology, New Series*, vol. III/25 (Springer, Heidelberg, 1991).
- ⁴⁴ W. Xu and J. B. Adams, *Surf. Sci.* **301**, 371 (1994), and references therein.
- ⁴⁵ M. Arnold, G. Hupfauer, P. Bayer, L. Hammer, K. Heinz, B. Kohler, and M. Scheffler, *Surf. Sci.* **382**, 288 (1997).
- ⁴⁶ H. L. Davis and G. C. Wang, *Bull. Amer. Phys. Soc.* **29**, 221 (1984).
- ⁴⁷ O. Grizzi, M. Shi, H. Bu, J. W. Rabalais, and P. Hochmann, *Phys. Rev. B* **40**, 10127 (1989).
- ⁴⁸ G. J. Ackland and R. Thetford, *Phil. Mag. A* **56**, 15 (1987).
- ⁴⁹ F. Ercolessi, O. Tomagnini, S. Iarlori, and E. Tosatti, in *Nanosources and Manipulation of Atoms Under High Fields and Temperatures: Applications*, edited by V. T. Binh (Kluwer, 1993), pp. 185–205.
- ⁵⁰ H. J. C. Berendsen, J. P. M. Postma, W. F. Gunsteren, A. D. Nola, and J. R. Haak, *J. Chem. Phys.* **81**, 3684 (1984).
- ⁵¹ W. Xu and J. B. Adams, *Surf. Sci.* **319**, 45 (1994), and references therein.
- ⁵² A. Larose and B. N. Brockhouse, *Can J. Phys.* **54**, 1819 (1976).
- ⁵³ D. C. Wallace, *Thermodynamics of Crystals* (Dover, Mineola, NY, 1998).
- ⁵⁴ R. Wyckoff, *Crystal Structures* (Interscience, New York, 1963), 2nd ed.
- ⁵⁵ K. Balasubramanian, *J. Chem. Phys.* **112**, 7425 (2000).
- ⁵⁶ S. Sickafoose, A. Smith, and M. Morse, *J. Chem. Phys.* **116**, 993 (2002).
- ⁵⁷ M. Lee and R. S. Gilmore, *J. Mater. Sci.* **17**, 2657 (1982).
- ⁵⁸ B. Predel, *Landolt-Börnstein: numerical data and functional relationships in science and technology, New Series*, vol. IV/5 B (Springer, Heidelberg, 1998).
- ⁵⁹ A. A. Rempel, R. Würschum, and H.-E. Schaefer, *Phys. Rev. B* **61**, 5945 (2000).
- ⁶⁰ G.-X. Qian, R. M. Martin, and D. J. Chadi, *Phys. Rev. B* **38**, 7649 (1988).
- ⁶¹ S. B. Zhang and J. E. Northrup, *Phys. Rev. Lett.* **67**, 2339 (1991).
- ⁶² D. J. Siegel, L. G. Hector, and J. B. Adams, *Surf. Sci.* **498**, 321 (2002).
- ⁶³ M. Christensen and G. Wahnström, *Phys. Rev. B* **67**, 115415 (2003).
- ⁶⁴ R. Frauenfelder, *J. Vac. Sci. Technol.* **6**, 388 (1969).
- ⁶⁵ Z. Ma and K. Balasubramanian, *Chem. Phys. Lett.* **181**, 467 (1991).
- ⁶⁶ K. Balasubramanian and Z. Ma, *J. Phys. Chem.* **95**, 9794 (1991).
- ⁶⁷ N. Balabanov and J. Boggs, *J. Phys. Chem. A* **104**, 7370 (2000).
- ⁶⁸ N. Tanpipat and J. Baker, *J. Phys. Chem.* **100**, 19818 (1996).
- ⁶⁹ M. Shen, H. F. Schaefer, and H. Partridge, *J. Chem. Phys.* **98**, 508 (1993).
- ⁷⁰ S. T. Picraux and F. L. Vook, *J. Nucl. Mater.* **53**, 246 (1974).
- ⁷¹ K. Nordlund, N. Runeberg, and D. Sundholm, *Nucl. Instr. Meth. Phys. Res. B* **132**, 45 (1997).
- ⁷² J. F. Ziegler, J. P. Biersack, and U. Littmark, *The Stopping and Range of Ions in Matter* (Pergamon, New York, 1985).